

Scattering of ${}^7\text{Be}$ and ${}^8\text{B}$ and the astrophysical S_{17} factor

G. Tabacaru,¹ A. Azhari,^{1,*} J. Brinkley,¹ V. Burjan,² F. Carstoiu,³ Changbo Fu,¹ C.A. Gagliardi,¹
V. Kroha,² A.M. Mukhamedzhanov,¹ X. Tang,^{1,†} L. Trache,¹ R.E. Tribble,¹ and S. Zhou⁴

¹*Cyclotron Institute, Texas A&M University, College Station, TX 77843*

²*Institute of Nuclear Physics, Czech Academy of Science, Prague-Rez, Czech Republic*

³*Institute of Physics and Nuclear Engineering H. Hulubei, Bucharest, Romania*

⁴*China Institute of Atomic Energy, P.O. Box 275(46), Beijing 102 413, P.R. China*

(Dated: November 13, 2018)

Measurements of scattering of ${}^7\text{Be}$ at 87 MeV on a melamine ($\text{C}_3\text{N}_6\text{H}_6$) target and of ${}^8\text{B}$ at 95 MeV on C were performed. For ${}^7\text{Be}$ the angular range was extended over previous measurements and monitoring of the intensity of the radioactive beam was improved. The measurements allowed us to check and improve the optical model potentials used in the incoming and outgoing channels for the analysis of existing data on the proton transfer reaction ${}^{14}\text{N}({}^7\text{Be}, {}^8\text{B}){}^{13}\text{C}$. The results lead to an updated determination of the asymptotic normalization coefficient for the virtual decay ${}^8\text{B} \rightarrow {}^7\text{Be} + p$. We find a slightly larger value, $C_{\text{tot}}^2({}^8\text{B}) = 0.466 \pm 0.047 \text{ fm}^{-1}$, for the melamine target. This implies an astrophysical factor, $S_{17}(0) = 18.0 \pm 1.8 \text{ eV}\cdot\text{b}$, for the solar neutrino generating reaction ${}^7\text{Be}(p,\gamma){}^8\text{B}$.

PACS numbers: 24.10.Ht; 25.60.Bx; 25.60.Je; 26.65.+t

I. INTRODUCTION

Measurements of the energetic neutrinos produced in ${}^8\text{B}$ beta decay have played a prominent role in our new understanding of neutrino properties (see [1, 2, 3, 4, 5] and references therein). ${}^8\text{B}$ is produced in the sun by the ${}^7\text{Be}(p,\gamma){}^8\text{B}$ reaction. A good understanding of this reaction rate is needed in order to calculate the expected neutrino flux in the standard solar model [4]. The determination of the astrophysical S_{17} factor has, therefore, been the subject of intense experimental and theoretical effort over the past decade. This work has been summarized in several recent publications [6, 7, 8]. In spite of these efforts, there is no clear consensus on the value of $S_{17}(0)$ at the desired 5% precision. Consequently, several new experiments are under way or planned.

We previously reported measurements of the asymptotic normalization coefficients (ANC) for ${}^8\text{B}$ using the proton transfer reactions ${}^{10}\text{B}({}^7\text{Be}, {}^8\text{B}){}^9\text{Be}$ [9] and ${}^{14}\text{N}({}^7\text{Be}, {}^8\text{B}){}^{13}\text{C}$ [10]. The ANCs determine the amplitude of the tail of the overlap integral of the ground state wave function of ${}^8\text{B}$ onto the two-body channel ${}^7\text{Be} + p$. To find the ANCs with the ${}^{14}\text{N}({}^7\text{Be}, {}^8\text{B}){}^{13}\text{C}$ transfer reaction, a distorted wave Born approximation (DWBA) calculation is carried out and compared to the measured data. The DWBA calculation needs optical model parameters (OMP) for both the incoming ${}^7\text{Be}+{}^{14}\text{N}$ and outgoing ${}^8\text{B}+{}^{13}\text{C}$ channels. Here we report a measurement of ${}^7\text{Be}$ elastic scattering on a melamine ($\text{C}_3\text{N}_6\text{H}_6$) target, where we doubled the angular range and improved the monitoring of the intensity of the ${}^7\text{Be}$ radioactive beam relative to our previous measurement [10]. The ex-

tension of the angular range was done to obtain a better determination of the optical potential in the incoming channel. We also measured the elastic scattering of a ${}^8\text{B}$ beam on a C target with the aim of checking, for the first time, the OMP that were used in the outgoing channel ${}^8\text{B}+{}^{13}\text{C}$.

Below we describe the radioactive beam production, the experimental setups, and the procedure for the data reduction. We then give results of calculations for optical potentials in both the incoming and outgoing channels based on a double folding procedure with an effective nucleon-nucleon interaction. We discuss the consequences of the improved secondary beam normalization, and compare revised DWBA calculations to the ${}^{14}\text{N}({}^7\text{Be}, {}^8\text{B}){}^{13}\text{C}$ data from Ref. [10] in order to extract a new value for the ANCs and the corresponding astrophysical factor S_{17} .

II. THE EXPERIMENTS

The ${}^7\text{Be}$ radioactive beam was produced and separated using the Momentum Achromatic Recoil Spectrometer (MARS) [11]. The primary beam was ${}^7\text{Li}$ at 18.6 MeV/A delivered by the K500 superconducting cyclotron at Texas A&M University. It bombarded a liquid nitrogen cooled H_2 gas target at a pressure of 2 atm, with entrance and exit windows of 12 μm thick Havar. A secondary beam of ${}^7\text{Be}$ at 12.5 MeV/A was filtered from other reaction products by MARS. The characteristics of the beam spot, which were measured with a 900 μm thick two-dimensional Position Sensitive Silicon Detector (PSSD) placed at the MARS focal plane (the target detector), were a spot size of 2.5 mm \times 3.6 mm FWHM (horizontal \times vertical) and an angular spread of $1.8^\circ \times 0.6^\circ$. The purity of the ${}^7\text{Be}$ beam was 99% at an average rate of $\sim 80 \text{ kHz}$. Alpha particles were

*Present address: Alix Partners, Dallas, TX

†Present address: Argonne National Laboratory, Argonne, IL

the primary contaminant. For a detailed description of radioactive beam production with MARS, see Ref. [12]. Following beam tuning, the secondary target, a melamine foil with a thickness of 1.5 mg/cm^2 , was moved into the beam spot. Four $5 \times 5 \text{ cm}^2$ PSSDs were placed symmetrically around the target on an aluminum plate, as shown in Fig. 1. Detectors 1 and 2 ($110 \text{ }\mu\text{m}$ thick) covered a laboratory angular range from 4° to 19° , and detectors 3 and 4 ($65 \text{ }\mu\text{m}$ thick) covered 16° to 30° . All four PSSDs were backed by $500 \text{ }\mu\text{m}$ thick silicon detectors providing particle identification spectra ($\Delta E, E$). Each PSSD was position calibrated using a mask with 6 slots that were 0.8 mm wide and were spaced 8 mm apart. The detectors were cooled to approximately -10°C with two electric thermocoolers fixed on the aluminum plate in order to decrease the inverse current in the detectors and minimize their noise. The assembly was placed on a XYZ optical table for precise positioning.

In our previous experiments with a ^7Be beam [9, 10], the number of secondary beam particles was determined indirectly by measuring the intensity of the ^7Li primary beam in a Faraday cup, and normalizing the yield at low primary beam intensities by counting the ^7Be with the target detector. Periodically (typically once a day) the calibration procedure was repeated to check for any rate variations due to drifts in MARS power supplies. The primary ^7Li beam intensity was substantially higher for the experiment on the melamine target [10] than the experiment on the ^{10}B [9] target.

Following these two measurements, we modified the experimental setup by adding a monitor detector to count the radioactive beam particles directly. The beam monitoring system, which is shown in Fig. 1, used a wire mesh screen to reduce the secondary beam intensity and a plastic scintillator coupled with a photomultiplier tube to count the radioactive beam particles that passed through the target. In parallel, we ran the old monitoring system with a Faraday cup for the primary beam, and compared the results. In subsequent measurements with a high-intensity ^{11}B primary beam, we observed a difference between the two normalization procedures. Beam heating reduced the density of the gas in the production target, causing a drop in the isotope production rate per nA of primary beam current and increasing the central beam energy.

By scaling the heat deposition of the beam in the gas target, we concluded that this effect may have produced a small but non-negligible shift in the beam normalization during the previous $^{14}\text{N}(^7\text{Be}, ^8\text{B})^{13}\text{C}$ experiment. The effect was to over estimate the number of secondary beam particles and hence reduce the cross section and the resulting ANC. In contrast, the primary beam intensity for the $^{10}\text{B}(^7\text{Be}, ^8\text{B})^9\text{Be}$ measurement was sufficiently low to have a negligible effect. For the present experiment, the monitor detector was a NE102A plastic scintillator coupled to a photomultiplier tube. To minimize rate-dependent effects in the photomultiplier tube, two screens with a transparency of 9% each were added

to attenuate the beam intensity. The yield in the monitor detector was calibrated using the procedure described in Ref. [13].

For the ^8B elastic scattering measurement, the radioactive beam was produced via the $^1\text{H}(^{10}\text{B}, ^8\text{B})^3\text{H}$ reaction using a 27 MeV/A ^{10}B primary beam on the same LN₂-cooled gas cell. The cell contained H₂ gas at 3 atm pressure, corresponding to a target thickness of $\approx 10.8 \text{ mg/cm}^2$. Entrance and exit windows were made of $50 \text{ }\mu\text{m}$ (42 mg/cm^2) Havar. A 137 mg/cm^2 Al degrader was placed behind the gas cell to reduce the secondary beam energy. A 95 MeV radioactive beam of ^8B was focused at the end of MARS with a rate of about 5 kHz . The beam purity was better than 95%, with α particles being the primary contaminant. The full-width energy spread was limited to 1.6 MeV using momentum defining slits. Beam emittance was optimized using a pair of slits after the last quadrupole in MARS. The plastic scintillator behind the target was used for direct counting of the secondary beam particles, in this case without any wire mesh screen. Two telescopes, each consisting of a $110 \text{ }\mu\text{m}$ thick PSSD backed by a $500 \text{ }\mu\text{m}$ thick Si detector, observed the secondary reaction products. The telescopes covered the angular range $\theta_{lab} = 4^\circ - 19^\circ$. A 1.9 mg/cm^2 C target was used for the elastic scattering measurement.

In both experiments, target properties such as thickness and uniformity were verified using the radioactive ^7Be and ^8B beams directly by detecting beam particles at 0° with and without the target. The resultant energy loss measurements were compared to calculations with the computer code SRIM [14] to extract the thicknesses.

III. RESULTS

A. ^7Be elastic scattering

There were two motivations for measuring elastic scattering of ^7Be from melamine. The new detector geometry allowed us to extend the angular region for elastics which, in turn, helps to define optical model parameters. Further, it allowed us to normalize the elastic scattering yield directly by counting ^7Be particles after the secondary target.

The kinematic reconstruction of the elastically scattered reaction products was performed using the energy and position information from the four detector telescopes. The events selected corresponded to elastic scattering of ^7Be on ^{14}N and ^{12}C since the two contributions could not be separated. First, we identified all the events with $(\Delta E, E)$ corresponding to ^7Be , then we utilized the correlation of ^7Be energy vs. scattering angle to select those that were consistent with elastic scattering off either ^{14}N or ^{12}C . This discriminated against scattering on H and inelastic scattering populating excited states in either ^{14}N or ^{12}C . However, it was not possible to separate the elastically scattered events from inelastic scattering leading to the first excited state in ^7Be at $E_{ex} = 0.429$

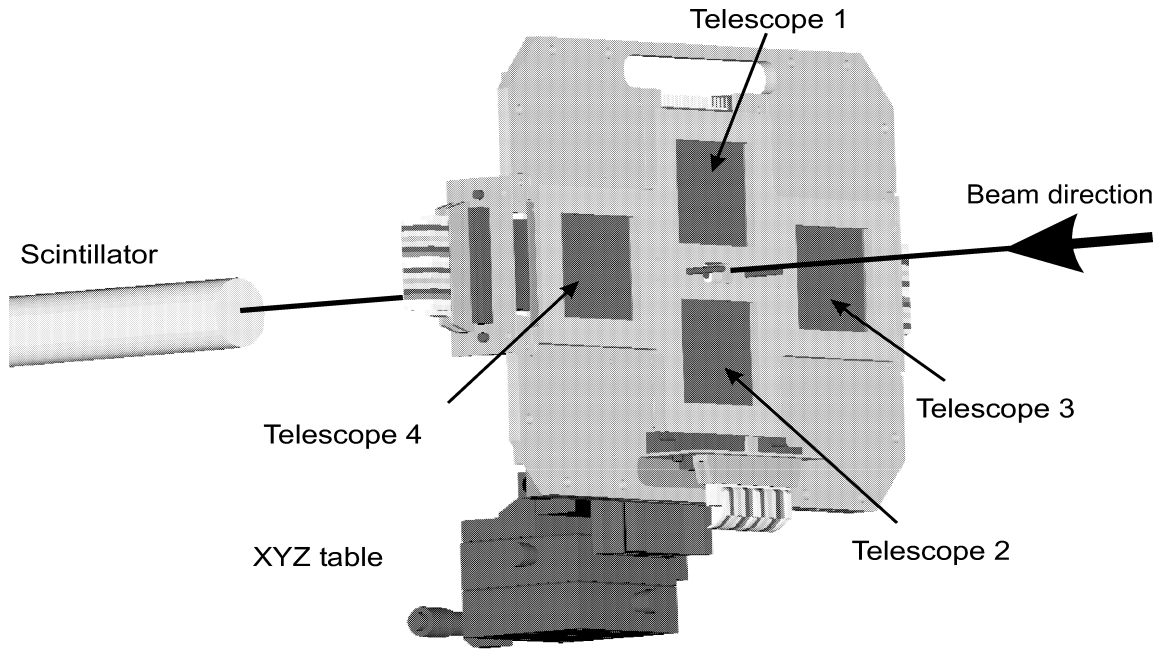


FIG. 1: A three-dimensional view of the detector assembly.

MeV. We estimated this contribution using data obtained from inelastic scattering of ${}^7\text{Li}$ on ${}^{13}\text{C}$ at 63 MeV [15] to the analog state at $E_{ex} = 0.477$ MeV. Assuming that the deformation lengths are equal for the analog states, we calculated the inelastic cross section for ${}^7\text{Be}$ on ${}^{14}\text{N}$ and ${}^{12}\text{C}$ at the current energy and subtracted it from the data. The correction was negligible at all but the largest angles, where it amounted to a few percent. The solid angle calculation as a function of scattering angle was done using a Monte Carlo simulation that took the measured properties of the beam spot and the geometrical specifications of the detector assembly as input data. The procedure has been described in previous publications (e.g. see Ref. [12]). Figure 2 shows the resulting angular distribution corresponding to elastically scattered ${}^7\text{Be}$ on ${}^{14}\text{N}$ and ${}^{12}\text{C}$.

The angular distribution predicted from the optical model parameters used in Ref. [12] is compared to the data in Fig. 2. The Monte Carlo calculation was used to provide the proper angular distribution that takes into account the finite angular binning in the data.

The results of our measurements are compatible with those reported in Ref. [10] at small angles and with the predictions of the optical model calculations done at that time (dotted curve). However, the new experimental data fall above the predictions at larger angles, suggesting a smaller absorption than was assumed in Ref. [10]. In order to obtain a better description of the elastic scattering, calculations were carried out with a range of new parameters. These were also used for the entrance channel to generate DWBA predictions for the ${}^{14}\text{N}({}^7\text{Be}, {}^8\text{B}){}^{13}\text{C}$ proton transfer reaction.

The optical parameters used in Ref. [10] were based

on results from an analysis of elastic scattering of loosely bound p -shell nuclei [16], which demonstrated that the data can be described with double-folded potentials. The potentials quoted in Ref. [16] were obtained from calculated nuclear matter densities folded with an effective nucleon-nucleon interaction (JLM, [17]), smeared (two range parameters, t_V and t_W) and renormalized (two strength parameters, N_V and N_W) to produce:

$$U_{DF}(r) = N_V V(r, t_V) + i N_W W(r, t_W). \quad (1)$$

The calculations for previous ${}^7\text{Be}$ studies were done using the JLM1 effective interaction with standard range parameters: $t_V=1.20$ fm, $t_W=1.75$ fm, and average renormalizations $N_V=0.37$, $N_W=1.00$ (for details see Ref. [16] and references therein). These parameters served as the starting point for the new calculations. Elastic scattering of ${}^7\text{Be}$ at 87.7 MeV on ${}^{14}\text{N}$ and ${}^{12}\text{C}$ were calculated in the center of mass frame, then transformed into the lab frame and added with weights 1.0 and 0.5, respectively, equal to the ratio of ${}^{14}\text{N}$ to ${}^{12}\text{C}$ nuclei in the melamine. The resulting curve was “smoothed” using the Monte Carlo code described above. The parameters for the folding potential were varied simultaneously and identically for both target nuclei. This approach is supported by the fact that both target nuclei are well bound and have similar densities in the surface region and by experiments we have carried out with melamine and C targets using other radioactive beams, such as ${}^{13}\text{N}$ [18], ${}^8\text{B}$ (present experiment) and ${}^{17}\text{F}$ [19]. The extended angular coverage of the present data was still not sufficient to attempt an optical model fit with free parameters. Rather, the two normalization and two range parameters were varied. The parameters for various calculations and the reduced χ^2

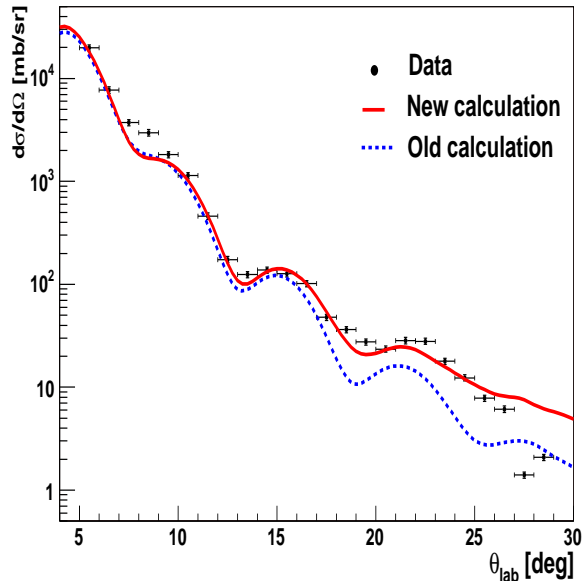


FIG. 2: (color online) Angular distribution for elastic scattering of ${}^7\text{Be}$ on ${}^{14}\text{N}$ and ${}^{12}\text{C}$. The points are experimental data after subtraction of the inelastic scattering contribution. The solid (red) line is the new calculation, and the dashed line (blue) is the previous calculation from Ref. [12]. Both calculations are smeared to account for the finite angular resolution.

values obtained by comparison to the data are presented in Table I.

Four entries in the Table (A, B, C and H) were obtained by adjusting the renormalization of the real and imaginary parts of the potential. The smearing ranges of the interaction, t_V and t_W , were adjusted for three cases (D, E, F), and the density dependence was adjusted in one case (G) where the JLM2 interaction was used. The best results were obtained for cases D, E, G and H. The small differences between the χ^2 values show that it is difficult to choose a “best solution”. Rather, we did DWBA calculations for the ${}^{14}\text{N}({}^7\text{Be}, {}^8\text{B}){}^{13}\text{C}$ transfer reaction for the four most promising potentials. The results are compared to the previous calculations in Table I.

A far/near decomposition of the scattering amplitudes shows that the observed angular range covers the region of Fraunhofer oscillations generated by the interference of the two components (see Fig. 3). Their crossover is around 20° , and at larger angles the far component becomes dominant. But in the region included in our measurements, the interference is still important. The calculations show that after about 60° the angular distributions develop a rainbow type pattern, typical for the cases found recently in our ${}^6,7\text{Li}$ elastic scattering data [20].

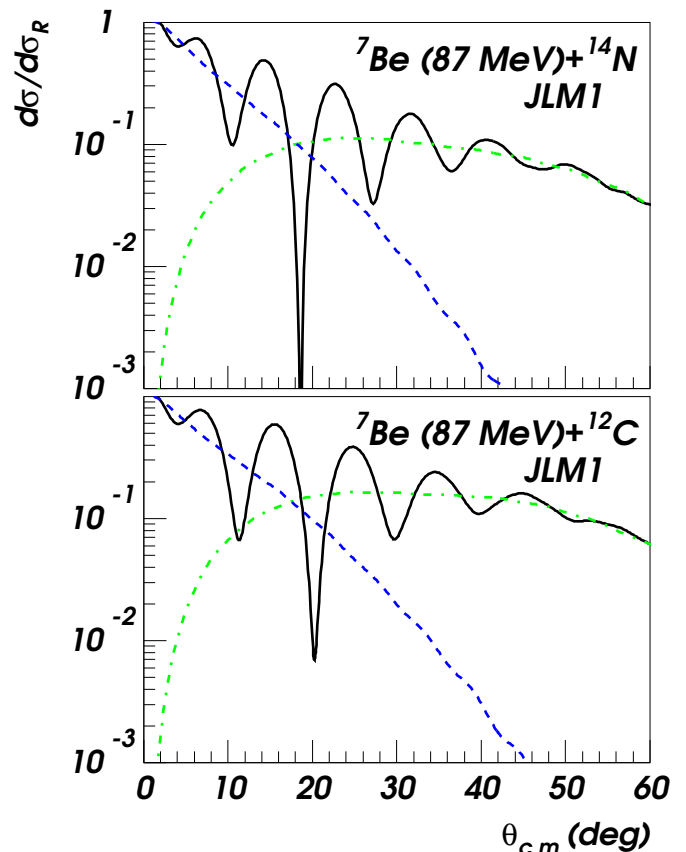


FIG. 3: (color online) Far side/near side components shown compared as ratios to Rutherford scattering for the potential H in Table I. The near side components are the dashed lines, the far side components are the dot-dashed lines, and the totals are given as the solid lines.

B. ${}^8\text{B}$ experiment

A similar analysis was used for the ${}^8\text{B}$ elastic scattering on a natural C target. The resulting angular distribution is shown in Fig. 4 where it is compared to calculations made with the folded potentials using the average parameters $t_V = 1.20$ fm, $t_W = 1.75$ fm, $N_V = 0.37$ and $N_W = 1.00$. The solid (dashed) line shows the results after (before) smoothing with the Monte Carlo calculation. The ${}^8\text{B}$ density used in the folding procedure was that calculated in [16] using the correct ANC for the last proton. Due to the limited angular range of the data, we did not attempt to produce a better fit by adjusting parameters. Based on the similar densities for ${}^{12}\text{C}$ and ${}^{13}\text{C}$ and on results found in cases where scattering on both ${}^{12}\text{C}$ and ${}^{13}\text{C}$ were measured, we assume that the parameters (t_V , t_W , N_V , N_W) extracted for the natural C target are valid for the ${}^8\text{B}+{}^{13}\text{C}$ channel in DWBA calculations of the transfer reaction.

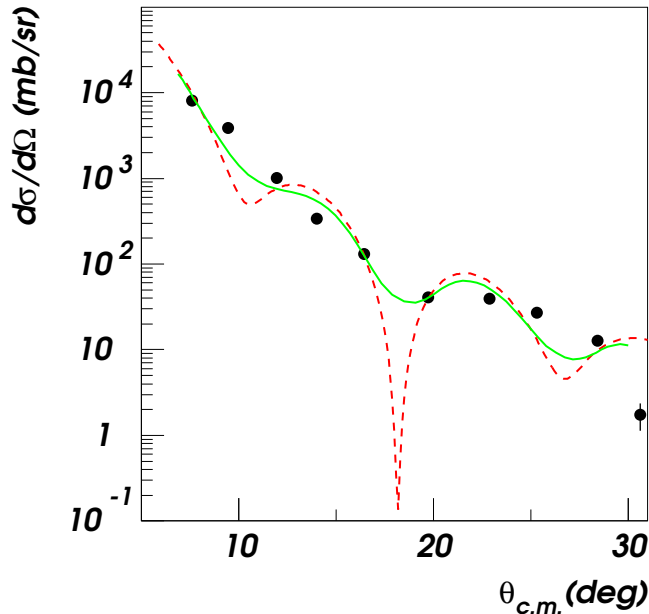


FIG. 4: (color online) The angular distribution for elastic scattering of ${}^8\text{B}$ on C . The dashed line is the calculated cross section and the solid line is the result after accounting for the finite angular resolution.

$$\begin{aligned} \frac{d\sigma}{d\Omega} = & C_{{}^8\text{B},p_{3/2}}^2 \left[\frac{C_{{}^{14}\text{N},p_{1/2}}^2}{b_{{}^{14}\text{N},p_{1/2}}^2} \frac{\sigma_{p_{1/2} \rightarrow p_{3/2}}}{b_{{}^8\text{B},p_{3/2}}^2} + \frac{C_{{}^{14}\text{N},p_{3/2}}^2}{b_{{}^{14}\text{N},p_{3/2}}^2} \frac{\sigma_{p_{3/2} \rightarrow p_{3/2}}}{b_{{}^8\text{B},p_{3/2}}^2} \right] \\ & + C_{{}^8\text{B},p_{1/2}}^2 \left[\frac{C_{{}^{14}\text{N},p_{1/2}}^2}{b_{{}^{14}\text{N},p_{1/2}}^2} \frac{\sigma_{p_{1/2} \rightarrow p_{1/2}}}{b_{{}^8\text{B},p_{1/2}}^2} + \frac{C_{{}^{14}\text{N},p_{3/2}}^2}{b_{{}^{14}\text{N},p_{3/2}}^2} \frac{\sigma_{p_{3/2} \rightarrow p_{1/2}}}{b_{{}^8\text{B},p_{1/2}}^2} \right] = C^2({}^8\text{B},p_{3/2}) [\tilde{\sigma}_{DW}] \end{aligned} \quad (2)$$

where the σ 's are the calculated DWBA differential cross sections for proton transfer from the $p_{3/2}$ and $p_{1/2}$ orbitals in ${}^{14}\text{N}$ to the $p_{3/2}$ and $p_{1/2}$ orbitals in ${}^8\text{B}$, the b_{lj} 's are the ANCs for the single particle orbitals used in the DWBA calculation, and the $C_{{}^{14}\text{N},lj}$'s and $C_{{}^8\text{B},lj}$'s are the ANCs for ${}^{14}\text{N} \rightarrow {}^{13}\text{C} + p$ and ${}^8\text{B} \rightarrow {}^7\text{Be} + p$, respectively. The ANCs, $C_{{}^{14}\text{N},p_{1/2}}^2 = 18.6(12) \text{ fm}^{-1}$ and $C_{{}^{14}\text{N},p_{3/2}}^2 = 0.93(14) \text{ fm}^{-1}$, were measured in [21, 22]. The calculations were done with the code PTOLEMY [23]. The results of the calculations are given in Table I where the value calculated and shown in column 7 is the quantity in the last square bracket in Eq. (2), $\tilde{\sigma}_{DW}$, integrated over the angular region $\theta_{c.m.} = 4^\circ - 25^\circ$ to match the data. This quantity contains the DWBA cross sections weighted with the ANCs for ${}^{14}\text{N}$, the single particle ANCs calculated for the appropriate Woods-Saxon proton binding potentials in ${}^8\text{B}$ and ${}^{14}\text{N}$ and the mixing ratio in the ground state of ${}^8\text{B}$, δ^2 . Since the reaction is periph-

IV. IMPLICATIONS FOR ${}^{14}\text{N}({}^7\text{Be}, {}^8\text{B}){}^{13}\text{C}$

Based on the present analysis, the value of the ${}^{14}\text{N}({}^7\text{Be}, {}^8\text{B}){}^{13}\text{C}$ proton transfer reaction cross section from our previous measurement ([10]) was increased, $\sigma_{exp}^{tr}(new) = 1.055 \sigma_{exp}^{tr}(old)$, to account for the difference of 5.5% found in the absolute normalization. Following the original publication the ratio between the ANCs for the $1p_{1/2}$ and $1p_{3/2}$ components in the wave function of the ground state of ${}^8\text{B}$ was found to be $\delta^2 = C^2({}^8\text{B}, p_{1/2}) / C^2({}^8\text{B}, p_{3/2}) = 0.125(20)$ from the mirror neutron transfer reaction ${}^{13}\text{C}({}^7\text{Li}, {}^8\text{Li}){}^{12}\text{C}$ [15]. The previous result had assumed $\delta^2 = 0.157$ based on theoretical calculations. The new cross section, the value of δ^2 from experiment, and the new optical model parameters have been used to find revised values of the ANCs for ${}^8\text{B} \rightarrow {}^7\text{Be} + p$ from the ${}^{14}\text{N}({}^7\text{Be}, {}^8\text{B}){}^{13}\text{C}$ proton transfer reaction measurement [10].

In order to extract the ANCs, four terms must be calculated to account for the possible proton transitions:

eral, the results do not depend on the geometry assumed for the proton binding potentials, which are chosen to be Woods-Saxon shape with depths adjusted to reproduce the experimental proton binding energies in ${}^8\text{B}$ and ${}^{14}\text{N}$, respectively. The results shown were calculated using the reduced radius $r_0 = 1.20 \text{ fm}$ and the diffuseness $a = 0.60 \text{ fm}$, and the same spin-orbit term as in Ref. [10]. The exit channel parameters were fixed to the previous values. Calculations were done at $E_{lab} = 83.5 \text{ MeV}$, the energy of the previous experiment with the four optical model sets in Table I for the entrance channel that have the lowest χ^2 , B, D, E, G, and H. In column 8 we give the ratio of the present calculations to the same quantity calculated in Ref. [10]. The average of the four results, weighted by the χ^2 's, gives the ratio $\langle \mathcal{R} \rangle = 0.968 \pm 0.047$. The new ANC, calculated with the relation

$$C_{{}^8\text{B},p_{3/2}}^2(new) = (1.055 / \langle \mathcal{R} \rangle) C_{{}^8\text{B},p_{3/2}}^2(old), \quad (3)$$

is $C_{sB,p_{3/2}}^2(\text{new}) = 0.414 \pm 0.041 \text{ fm}^{-1}$. The overall uncertainty contains contributions from statistics (2.6%), absolute normalization of the cross section (5%), input parameters in the Monte Carlo simulation of the experiment (1.4%), and uncertainties in the ANC for the ^{14}N vertex (6.4%). The contribution of each of these factors remains the same as in the original analysis [10]. The uncertainty due to the optical model parameters was taken from the standard deviation of the calculated cross sections (column 7 or 8 in Table I) and is 5% compared with the previous value of 8.1%.

The relation between the ANCs and the astrophysical factor $S_{17}(0)$, in eV·b, is [24]

$$S_{17}(0) = 38.6 \left(C_{p_{3/2}}^2 + C_{p_{1/2}}^2 \right) = 38.6 C_{p_{3/2}}^2 (1 + \delta^2) \quad (4)$$

Using the new value of the ANC we find $S_{17}(0) = 18.0 \pm 1.8 \text{ eV}\cdot\text{b}$. This value is very close to the value obtained from the reaction $^{10}\text{B}(^7\text{Be},^8\text{B})^9\text{Be}$ in Ref. [9] where we found $S_{17}(0) = 18.4 \pm 2.5 \text{ eV}\cdot\text{b}$. The weighted average of the two results is $S_{17}(0) = 18.2 \pm 1.7 \text{ eV}\cdot\text{b}$.

V. CONCLUSION

Elastic scattering of ^7Be at about 12 MeV/A has been measured over an extended angular range on a melamine target. The results provide a better determination of the optical model parameters used for the entrance channel of the $^{14}\text{N}(^7\text{Be},^8\text{B})^{13}\text{C}$ reaction. For the first time elastic scattering of ^8B was measured on a C target, thus allowing for a check the optical model parameters used for the exit channel in the DWBA calculation. In the measurement of the ^7Be elastic scattering, we directly counted the secondary beam particles. This resulted in a 5.5% increase of the transfer reaction cross section from Ref. [10], which used an indirect method to obtain the secondary beam intensity. We also used the mixing ratio between the $1p_{1/2}$ and $1p_{3/2}$ components from a ($^7\text{Li},^8\text{Li}$)

measurement [15], rather than a theoretical prediction. These improvements lead to the revised value of the ANC for $^8\text{B} \rightarrow ^7\text{Be} + p$ from the $^{14}\text{N}(^7\text{Be},^8\text{B})^{13}\text{C}$ reaction of $C^2(^8\text{B}, p_{3/2}; \text{new}) = 0.414 \pm 0.041 \text{ fm}^{-1}$, resulting in $C_{\text{tot}}^2(^8\text{B}; \text{new}) = C_{p_{3/2}}^2 + C_{p_{1/2}}^2 = 0.466 \pm 0.047 \text{ fm}^{-1}$. This, in turn leads to a larger value for the astrophysical S factor for the $^7\text{Be}(p,\gamma)^8\text{B}$ reaction, $S_{17}(0) = 18.0 \pm 1.8 \text{ eV}\cdot\text{b}$. This new value is very close to the one from the same reaction on the ^{10}B target [9]. Averaging the two results, we obtain $S_{17}(0) = 18.2 \pm 1.7 \text{ eV}\cdot\text{b}$ from the proton transfer reactions.

Our result for $S_{17}(0)$ is a bit over 2σ lower than the extrapolation of the most recent and precise direct measurement of $^7\text{Be}(p,\gamma)^8\text{B}$ by Junghans *et al.* [7]. Our central value is about 1.5σ lower than the average central value obtained by Cyburt *et al.* [8] in a recent analysis that uses all of the best available capture data, under the assumption that they are independent. Including the uncertainty quoted by Cyburt *et al.* our results are consistent at the 1σ level. We do not understand the reason for the discrepancy between our ANC result and the extrapolated value from Junghans *et al.*. However, we note that direct measurements with both radioactive beams and targets and indirect measurements continue to be carried out on this important proton capture reaction.

Acknowledgments

This work was supported in part by the U.S. Department of Energy under Grant No. DE-FG03-93ER40773, the U.S. National Science Foundation under Grant No. INT-459521-00001, the Romanian Ministry for Education, Research and Youth under contract no. 555/2000, and the Robert A. Welch Foundation. One of the authors (F.C.) acknowledges the support of the Cyclotron Institute, Texas A&M University for part of the time this work was done.

-
- [1] R. Davis, D. Harmer, and K. C. Hoffman, Phys. Rev. Lett **20**, 1205 (1968).
[2] S. Fukuda et al. (Super-Kamiokande collaboration), Phys. Rev. Lett **86**, 5651 (2001).
[3] S. N. Ahmed et al. (SNO collaboration), Phys. Rev. Lett **87**, 071301 (2003).
[4] J. Bahcall and M. Pinsonneault, Phys. Rev. Lett **92**, 121301 (2004).
[5] W. Haxton, P. Parker, and C. Rolfs, arxiv:nucl-th/0501020 (2005).
[6] B. Davids and S. Typel, Phys. Rev. C **68**, 045802 (2003).
[7] A. R. Junghans, E. C. Mohrmann, K. A. Snover, T. D. Steiger, E. G. Adelberger, J. M. Casandjian, H. E. Swanson, L. Buchmann, S. H. Park, et al., Phys. Rev. C **68**, 065803 (2003).
[8] R. H. Cyburt, B. Davids, and B. K. Jennings, Phys. Rev. C **70**, 045801 (2004).
[9] A. Azhari, V. Burjan, F. Carstoiu, H. Dejbakhsh, C. Gagliardi, V. Kroha, A. Mukhamedzhanov, L. Trache, and R. Tribble, Phys. Rev. Lett. **82**, 3960 (1999).
[10] A. Azhari, V. Burjan, F. Carstoiu, C. A. Gagliardi, V. Kroha, A. M. Mukhamedzhanov, X. Tang, L. Trache, and R. E. Tribble, Phys. Rev. C **60**, 055803 (1999).
[11] R. E. Tribble, A. Azhari, C. A. Gagliardi, J. C. Hardy, A. M. Mukhamedzhanov, X. Tang, L. Trache, and S. J. Yennello, Nucl. Phys. A **701**, 278C (2002).
[12] A. Azhari, V. Burjan, C. Gagliardi, V. Kroha, A. Mukhamedzhanov, F. Nunes, X. Tang, L. Trache, and R. Tribble, Phys. Rev. C **63**, 055803 (2001).
[13] X. Tang, A. Azhari, C. Gagliardi, A. Mukhamedzhanov, F. Pirlpesov, L. Trache, R. Tribble, V. Burjan, V. Kroha, and F. Carstoiu, Phys. Rev. C **67**, 015804

TABLE I: The optical model parameters, the corresponding χ^2 per degree of freedom for the ^7Be elastic scattering fits, the calculated DWBA cross section for the $^{14}\text{N}(^7\text{Be}, ^8\text{B})^{13}\text{C}$ reaction (see text), and the ratio of the calculated DWBA calculation to that in Ref. [10].

| Calculation | N_V | N_W | t_V [fm] | t_W [fm] | χ^2/N | $\tilde{\sigma}_{DW}$ | Ratio $\mathcal{R} = \frac{\sigma_{DW}(new)}{\sigma_{DW}(orig)}$ |
|-------------|-------|-------|------------|------------|------------|-----------------------|---|
| Ref. [10] | 0.37 | 1.00 | 1.20 | 1.75 | 35.19 | 2.469 | 1.000 |
| A | 0.45 | 0.90 | 1.20 | 1.75 | 10.72 | | |
| B | 0.40 | 0.92 | 1.20 | 1.75 | 15.02 | 2.385 | 0.966 |
| C | 0.42 | 0.92 | 1.20 | 1.75 | 12.84 | | |
| D | 0.42 | 0.90 | 0.80 | 1.75 | 10.31 | 2.408 | 0.975 |
| E | 0.42 | 0.90 | 0.80 | 1.55 | 7.97 | 2.538 | 1.028 |
| F | 0.52 | 0.78 | 0.12 | 2.59 | 25.72 | | |
| G | 0.40 | 0.85 | 1.20 | 1.75 | 7.49 | 2.375 | 0.962 |
| H | 0.40 | 0.85 | 1.20 | 1.75 | 9.22 | 2.137 | 0.900 |

(2003).

- [14] J. F. Ziegler, J. P. Biersack, and U. Littmark, *The Stopping and Ranges of Ions in Matter, Vol I: The Stopping and Range of Ions in Solids* (Pergamon Press, New York, 1985).
- [15] L. Trache, A. Azhari, F. Carstoiu, H. L. Clark, C. A. Gagliardi, Y.-W. Lui, A. M. Mukhamedzhanov, X. Tang, N. Timofeyuk, and R. E. Tribble, Phys. Rev. C **67**, 062801(R) (2003).
- [16] L. Trache, A. Azhari, H. L. Clark, C. A. Gagliardi, Y.-W. Lui, A. M. Mukhamedzhanov, R. E. Tribble, and F. Carstoiu, Phys. Rev. C **61**, 024612 (2000).
- [17] J. P. Jeukenne, A. Lejeune, and C. Mahaux, Phys. Rev. C **16**, 80 (1977).
- [18] X. Tang, A. Azhari, C. Fu, C. A. Gagliardi, A. M. Mukhamedzhanov, F. Pirlpesov, L. Trache, R. E. Tribble, V. Burjan, V. Kroha, et al., Phys. Rev. C **69**, 055807 (2004).
- [19] J. Blackmon, D. Bardayan, C. Brune, F. Carstoiu, A. Champagne, R. Crespo, T. Davinson, J. Fernandes, C. Gagliardi, and U. G. et al., Nucl. Phys. A **746**, 365 (2004).
- [20] F. Carstoiu and L. Trache and R. E. Tribble and C. A. Gagliardi, Phys. Rev. C **70**, 054610 (2004).
- [21] L. Trache, A. Azhari, H. L. Clark, C. A. Gagliardi, Y. W. Lui, A. M. Mukhamedzhanov, R. E. Tribble, and F. Carstoiu, Phys. Rev. C **58**, 2715 (1998).
- [22] P. Bem, V. Burjan, V. Kroha, J. Novak, S. Piskor, E. Simeckova, J. Vincour, C. A. Gagliardi, A. M. Mukhamedzhanov, and R. E. Tribble, Phys. Rev. C **62**, 024320 (2000).
- [23] M. Rhoades-Brown, M. H. Mcfarlane, and S. C. Pieper, Phys. Rev. C **21**, 2417 (1980).
- [24] H. M. Xu, C. A. Gagliardi, R. E. Tribble, A. M. Mukhamedzhanov, and N. K. Timofeyuk, Phys. Rev. Lett. **73**, 2027 (1994).